AUT Journal of Mechanical Engineering

AUT J. Mech. Eng., 3(1) (2019) 63-76
DOI: 10.22060/ajme.2018.14453.5728

Analytical Solution and Optimization for Energy Harvesting from Nonlinear Vibration of Magneto- Electro- Elastic Plate

H. Shorakaei[1], A.R. Shooshtari[1*], H.R. Karami[2]

[1] Department of Mechanical Engineering, Faculty of Engineering, Bu-Ali Sina University, Hamedan, Iran
[2] Department of Electrical Engineering, Faculty of Engineering, Bu-Ali Sina University, Hamedan, Iran

ABSTRACT: In the present paper, a mathematical model has been provided for a Magneto-Electro-Elastic (MEE) plate to investigate its energy harvesting in nonlinear transverse vibration. The nonlinear equations of motion of an MEE plate have been used based on the Kirchhoff plate theory. These equations have been reduced to an ordinary differential equation using the Airy stress function and Galerkin Method. Also, two other equations have been made using electrical and magnetic aspects of the structure. Then, the equivalent electrical and magnetic circuit of the structure is developed. There are three ordinary differential equations that need to be solved together. A closed-form solution has been obtained for the output power of the harvester using the method of multiple scales. The obtained results are compared with those of FEM and a good agreement observed between the results of displacement and voltage. By introducing an analytical relation for the power as a cost function, the Genetic Algorithm method is applied to optimize the best parameters of the harvester which gives the maximum power. The effect of various parameters of the harvester, such as dimension and thickness, on the power is investigated and the results are discussed.

Review History:
Received: 15 May 2018
Revised: 9 July 2018
Accepted: 7 September 2018
Available Online: 11 October 2019

Keywords:
Nonlinear vibration
Plate
Smart material
Magneto-electro-elastic
Optimization

1- Introduction

Harvesting of the energy from the vibration of structures, as a harmful phenomenon in the structural engineering, is one of the interesting subjects for scientists and researchers. There are different methods to harvest energy from vibration, but one of the main methods is to use smart materials, such as piezoelectric. One of the innovative smart materials which can convert the mechanical strains of the structures in electrical and magnetic fields, is the multiphase material of Magneto-Electro-Elastic (MEE). Based on this important property, this kind of smart materials can give more efficiency in energy harvesting. Deriving an analytical model for the Smart Materials Structures (SMS) can be helpful in designing smart devices. SMS can be used as an energy generator, which convert the environment energy into electric energy with more applications. The environment energy can be modeled as a harmonic excitation force, and the structure reacts as a vibration system.

In the literature, Zhang et al. [1] analyzed Magneto-Electric (ME) materials theoretically for collecting magnetic energy and converting it to electric energy. They also studied time-harmonic vibrations of a laminated ME plate of piezoelectric and piezomagnetic layers driven by a magnetic field. Rupp et al. [2] presented a topology optimization of energy harvesting devices using piezoelectric materials under the Finite Element Model (FEM). In this paper, both elastic materials and piezoelectric materials are considered for the design of energy harvesting devices under the topology optimization formulation. Junior et al. [3] showed an electromechanical Finite Element (FE) plate model for piezoelectric energy harvesting. Since piezoelectric energy harvesters was designed and manufactured as thin structures, the classical plate theory was employed in the formulation. Erturk et al. [4] introduced a piezomagnetoelastic device for substantial enhancement of piezoelectric power generation in vibration energy harvesting. Dai et al. [5] presented an energy harvester to convert ambient mechanical vibration into electrical energy employing the Terfenol-D/PZT/Terfenol-D laminate ME transducer. An analytical model is developed by them to analyze the nonlinear vibration and electrical-output performances of the harvester. They also fabricated and tested a prototype. Sun and Kim [6] concerned with the development of a systematic design method of MEE composites with maximized conversion of mechanical energy to electric and/or magnetic energy. They assumed a composite plate as simply supported and discretized it into a number of laminates for analysis using a semi-analytic finite element method. An equivalent single-layer model for the free vibration analysis of smart laminated plates is presented by Milazzo and Orlando [7]. The Excitation-Induced Stability (EIS) phenomenon in a harmonically excited bistable Duffing oscillator is studied by Wu et al. [8]. Design of plate structures for vibration energy harvesting from two or more vibration modes has been investigated by El-Hebeary et al. [9]. Stanton et al. [10] applied the method of harmonic balance to analytically predict the existence, stability, and influence of parameter variations on the Intrawell and interwell oscillations of bistable piezoelectric inertial generator. Talleb and Ren [11] presented the finite element analysis of a ME energy harvester using a laminate composite constituted of laminated piezoelectric and magnetostrictive layers. In this

Corresponding author, E-mail: shooshta@basu.ac.ir

study, both the nonlinear characteristics of the material and the dependency on the load impedance are considered. Ke and Wang [12] investigated the free vibration of MEE nanobeams based on the nonlocal theory of elasticity and Timoshenko beam theory. In this study, the MEE nanobeam is subjected to the external electric potential, magnetic potential and uniform temperature rise. Razavi and Shooshtari [13] studied nonlinear free vibration of symmetric magneto-electro-elastic laminated rectangular plates with simply supported boundary condition. They used the first order shear deformation theory, and considering the von Karman's nonlinear strains obtained the equations of motion, whereas Maxwell equations for electrostatics and magnetostatics are used to model the electrical and magnetic behavior of the plate. Shirbani et al. [14] proposed a coupled magneto-electro-mechanical (MEM) lumped parameter model for the response of the proposed MEE energy harvesting systems under base excitation. Shorakaei and Shooshtari [15] studied analytical solution and energy harvesting from nonlinear vibration of an asymmetric bimorph piezoelectric plate and optimized the plate parameters by genetic algorithm.

In this paper, an analytical nonlinear model for a bimorph MEE plate is developed for the first time. The equivalent electrical and magnetic circuits are presented for the provided model. The nonlinear governing equations based on the Kirchhoff's plate theory and von-Karman's nonlinear strains are solved using multiple scales method, simultaneously with two electromagnetic coupled equations. The analytical relations for electrical voltage, induced current and output power are obtained, as well. By assuming power relation as cost function, some parameters of the harvester are optimized using genetic algorithm, in that way the output power can reach to maximum value.

2- Governing Equation

Fig. 1 shows a MEE plate connected to a resistance load *R*. This structure includes two MEE layers with equal thickness in top and bottom of the substructure and it is excited by a harmonic force. In order to convert the magnetic field into electrical current, two coils have been considered in two side of the structure however they have not been shown in the schematic picture. The parameters *a* and *b* are width and length of the plate and h_s and h_i are the thickness of the substructure and MEE layers, respectively. The origin of the coordinate system is considered to be in one of the corners of the plate's mid-plane. The plate is considered to be thin with length to thickness ratio $a/h>20$, so that the classical plate theory can be used [16]. In the recent equation h is the thickness of the plate and is defined $h=2h_i+h_s$.

2- 1- Stain and displacement field

Based on Kirchhoff theory, following displacement field is used

$$\begin{cases} u(x,y,z) = u_0(x,y,z) - z\dfrac{\partial w_0}{\partial x} \\ v(x,y,z) = v_0(x,y,z) - z\dfrac{\partial w_0}{\partial y} \\ w(x,y,z) = w_0(x,y,z) \end{cases} \tag{1}$$

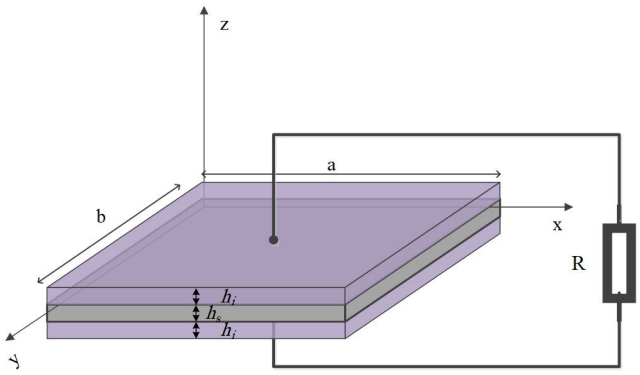

Fig. 1. Schematic of the magnetoelectroelastic plate connected to the resistance load *R*.

where (u_0,v_0,w_0) denotes the displacements of a material point at $(x,y,0)$ in (x,y,z) coordinate directions. (u_0,v_0) is associated to the extensional deformation of the plate while w_0 denotes the bending deflection [17]. For the given displacement field in Eq. (1) the strains are defined as Eq. (2)

$$\begin{Bmatrix} \varepsilon_{xx} \\ \varepsilon_{yy} \\ \varepsilon_{xy} \end{Bmatrix} = \begin{Bmatrix} \varepsilon^0_{xx} \\ \varepsilon^0_{yy} \\ \varepsilon^0_{xy} \end{Bmatrix} + z \begin{Bmatrix} \varepsilon^1_{xx} \\ \varepsilon^1_{yy} \\ \varepsilon^1_{xy} \end{Bmatrix} \tag{2}$$

Transverse strains in *z* direction is zero approximately [18]. The relations between strain and displacement are introduced as following form

$$\begin{cases} \varepsilon^0_{xx} = \dfrac{\partial u_0}{\partial x} + \dfrac{1}{2}\left(\dfrac{\partial w_0}{\partial x}\right)^2 \\ \varepsilon^0_{yy} = \dfrac{\partial v_0}{\partial y} + \dfrac{1}{2}\left(\dfrac{\partial w_0}{\partial y}\right)^2 \\ \varepsilon^0_{xy} = \dfrac{1}{2}\left(\dfrac{\partial u_0}{\partial y} + \dfrac{\partial v_0}{\partial x} + \dfrac{\partial w_0}{\partial x}\dfrac{\partial w_0}{\partial y}\right) \end{cases}, \begin{cases} \varepsilon^1_{xx} = -\dfrac{\partial^2 w_0}{\partial x^2} \\ \varepsilon^1_{yy} = -\dfrac{\partial^2 w_0}{\partial y^2} \\ \varepsilon^1_{xy} = -\dfrac{\partial^2 w_0}{\partial x\,\partial y} \end{cases} \tag{3}$$

The introduced strains in Eq. (3) are known as *von Karman* strains in which $\{\varepsilon^0\}$ is membrane strain and $\{\varepsilon^1\}$ is bending strain. One can see the von Karman strains terms are nonlinear terms which are necessary for nonlinear analysis of the harvesters.

Constituent equation of a MEE material layer is

$$\{\sigma\} = [Q]\{\varepsilon - \alpha\Delta T\} - [e]\{E\} - [q]\{H\} \tag{4-a}$$

$$\{D\} = [e]^T\{\varepsilon - \alpha\Delta T\} + [\in]\{E\} + [d]\{H\} \tag{4-b}$$

$$\{B\} = [q]^T\{\varepsilon - \alpha\Delta T\} + [d]\{E\} + [\mu]\{H\} \tag{4-c}$$

in which $\{\sigma\}$ $\{B\}$ and $\{D\}$, are the vectors of stress, electric displacement and magnetic flux density, respectively. $\{\varepsilon\}$, $\{E\}$ and $\{H\}$ are strain, electric field and intensity of a magnetic field vectors, respectively.

[Q], [$\in$] and also [μ] are coefficient matrices of elastic, dielectric and permittivity, respectively. [e], [q] and [d] are the coefficient matrices of piezoelectric, piezomagnetic and electromagnetic. $\{\alpha\}$ and ΔT are thermal expansion vector and temperature change, respectively. Superscript T denotes transpose of the matrix. The detailed of above matrices are

$$Q=\begin{bmatrix} Q_{11} & Q_{12} & 0 \\ Q_{12} & Q_{22} & 0 \\ 0 & 0 & Q_{66} \end{bmatrix}, e=\begin{bmatrix} 0 & 0 & 0 \\ 0 & 0 & 0 \\ e_{31} & e_{32} & 0 \end{bmatrix},$$
$$\in=\begin{bmatrix} \in_{11} & 0 & 0 \\ 0 & \in_{22} & 0 \\ 0 & 0 & \in_{33} \end{bmatrix}, \alpha=\begin{Bmatrix} \alpha_1 \\ \alpha_2 \\ 0 \end{Bmatrix}, q=\begin{bmatrix} 0 & 0 & 0 \\ 0 & 0 & 0 \\ q_{31} & q_{32} & 0 \end{bmatrix}, \quad (5)$$
$$d=\begin{bmatrix} d_{11} & 0 & 0 \\ 0 & d_{22} & 0 \\ 0 & 0 & d_{33} \end{bmatrix}, \mu=\begin{bmatrix} \mu_{11} & 0 & 0 \\ 0 & \mu_{22} & 0 \\ 0 & 0 & \mu_{33} \end{bmatrix}$$

Here, a linear distribution of the electric and magnetic potential is assumed in the thickness direction (z). The z direction electric field, E_z is remarkable compared with the other directions [19] and are defined as

$$E_z=-\frac{V_e(t)}{h_i} \quad (6)$$

The relation of magnetic field intensity in the z direction, H_z, relation is transformed into electric current by two inducers in two sides of the structure in following form:

$$H_z=\frac{\bar{N}I_m(t)}{l} \quad (7)$$

In the above, $v_e(t)$ is the generated voltage by electrical part of the structure, $\bar{N}$ is the number of the coil, l is the length of the coil and $I_m(t)$ is the induced current by the magnetic field.

2- 2- Equations of motion

Using Hamilton's principle, motion equations of a plate based on classical theory and von-Karman strain-displacement relation are obtained as [20]:

$$\frac{\partial N_{xx}}{\partial x}+\frac{\partial N_{xy}}{\partial y}=I_0\frac{\partial^2 u_0}{\partial t^2}-I_1\frac{\partial^2}{\partial t^2}\left(\frac{\partial w_0}{\partial x}\right) \quad (8\text{-a})$$

$$\frac{\partial N_{xy}}{\partial x}+\frac{\partial N_{yy}}{\partial y}=I_0\frac{\partial^2 v_0}{\partial t^2}-I_1\frac{\partial^2}{\partial t^2}\left(\frac{\partial w_0}{\partial y}\right) \quad (8\text{-b})$$

$$\frac{\partial^2 M_{xx}}{\partial x^2}+2\frac{\partial^2 M_{xy}}{\partial x\,\partial y}+\frac{\partial^2 M_{yy}}{\partial y^2}+\frac{\partial}{\partial x}\left(N_{xx}\frac{\partial w_0}{\partial x}+N_{xy}\frac{\partial w_0}{\partial y}\right)+\frac{\partial}{\partial y}\left(N_{xy}\frac{\partial w_0}{\partial x}+N_{yy}\frac{\partial w_0}{\partial y}\right)+q(x,y,t)=I_0\frac{\partial^2 w_0}{\partial t^2}+I_1\frac{\partial^2}{\partial t^2}\left(\frac{\partial u_0}{\partial x}+\frac{\partial v_0}{\partial y}\right)-I_2\frac{\partial^2}{\partial t^2}\left(\frac{\partial^2 w_0}{\partial x^2}+\frac{\partial^2 w_0}{\partial y^2}\right) \quad (8\text{-c})$$

where q is external excitation, I_{is} for i=1,2,3 are mass moment inertias by which introducing N as number of layers, and h_k as the vertical position of the layers, can be expressed as:

$$\begin{Bmatrix} I_0 \\ I_1 \\ I_2 \end{Bmatrix}=\sum_{k=1}^{N}\int_{h_k}^{h_{k+1}}\begin{Bmatrix} 1 \\ z \\ z^2 \end{Bmatrix}\rho dz \quad (9)$$

and N_{xx}, N_{yy}, N_{xy} are in plane forces and M_{xx}, M_{yy}, M_{xy} are moments. In-plane forces and the moments can be expressed as:

$$\begin{Bmatrix} N_{xx} \\ N_{yy} \\ N_{xy} \end{Bmatrix}=\sum_{k=1}^{N}\int_{h_k}^{h_{k+1}}\begin{Bmatrix} \sigma_{xx} \\ \sigma_{yy} \\ \sigma_{xy} \end{Bmatrix}dz \quad (10)$$

$$\begin{Bmatrix} M_{xx} \\ M_{yy} \\ M_{xy} \end{Bmatrix}=\sum_{k=1}^{N}\int_{h_k}^{h_{k+1}}\begin{Bmatrix} \sigma_{xx} \\ \sigma_{yy} \\ \sigma_{xy} \end{Bmatrix}zdz \quad (11)$$

By substituting Eqs. (2) and (4)-a and (5) in Eqs. (10) and (11) one can obtain

$$\begin{Bmatrix} N_{xx} \\ N_{yy} \\ N_{xy} \end{Bmatrix}=\begin{bmatrix} A_{11} & A_{12} & 0 \\ A_{12} & A_{22} & 0 \\ 0 & 0 & A_{66} \end{bmatrix}\begin{Bmatrix} \varepsilon^0_{xx} \\ \varepsilon^0_{yy} \\ \varepsilon^0_{xy} \end{Bmatrix}+\begin{bmatrix} B_{11} & B_{12} & 0 \\ B_{12} & B_{22} & 0 \\ 0 & 0 & B_{66} \end{bmatrix}\begin{Bmatrix} \varepsilon^1_{xx} \\ \varepsilon^1_{yy} \\ \varepsilon^1_{xy} \end{Bmatrix}-\begin{Bmatrix} N^T_{xx} \\ N^T_{yy} \\ N^T_{xy} \end{Bmatrix}-\begin{Bmatrix} N^e_{xx} \\ N^e_{yy} \\ N^e_{xy} \end{Bmatrix}-\begin{Bmatrix} N^m_{xx} \\ N^m_{yy} \\ N^m_{xy} \end{Bmatrix} \quad (12)$$

$$\begin{Bmatrix} M_{xx} \\ M_{yy} \\ M_{xy} \end{Bmatrix}=\begin{bmatrix} B_{11} & B_{12} & 0 \\ B_{12} & B_{22} & 0 \\ 0 & 0 & B_{66} \end{bmatrix}\begin{Bmatrix} \varepsilon^0_{xx} \\ \varepsilon^0_{yy} \\ \varepsilon^0_{xy} \end{Bmatrix}+\begin{bmatrix} \bar{D}_{11} & \bar{D}_{12} & 0 \\ \bar{D}_{12} & \bar{D}_{22} & 0 \\ 0 & 0 & \bar{D}_{66} \end{bmatrix}\begin{Bmatrix} \varepsilon^1_{xx} \\ \varepsilon^1_{yy} \\ \varepsilon^1_{xy} \end{Bmatrix}-\begin{Bmatrix} M^T_{xx} \\ M^T_{yy} \\ M^T_{xy} \end{Bmatrix}-\begin{Bmatrix} M^e_{xx} \\ M^e_{yy} \\ M^e_{xy} \end{Bmatrix}-\begin{Bmatrix} M^m_{xx} \\ M^m_{yy} \\ M^m_{xy} \end{Bmatrix} \quad (13)$$

Stress can be expressed by Eq. (4a), where

$$\left(A_{ij},B_{ij},\bar{D}_{ij}\right)=\sum_{k=1}^{N}\int_{-\frac{h}{2}}^{\frac{h}{2}}[Q]\left(1,z,z^2\right)dz \quad (14)$$

$$\left\{N^T,M^T\right\}=\sum_{k=1}^{N}\int_{-\frac{h}{2}}^{\frac{h}{2}}(1,z)[Q]\{\alpha\}\Delta T dz \quad (15)$$

$$\left\{N^e,M^e\right\}=\sum_{k=1}^{N}\int_{-\frac{h}{2}}^{\frac{h}{2}}(1,z)[e]\{E\}dz \quad (16)$$

$$\left\{N^{m}, M^{m}\right\}=\sum_{k=1}^{N}\int_{-\frac{h}{2}}^{\frac{h}{2}}(1,z)[q]\{H\}dz \tag{17}$$

Since the structure is assumed to be symmetric in the z direction, so $B_{ij}=O_{3\times3}$ where is a 3×3 zero matrix. As axial deflection in x and y directions compared to z direction are so small, the acceleration term in both in-plane motions ($\partial^2u_0/\partial t^2$ and $\partial^2v_0/\partial t^2$) are neglected [21]. Also, the rotary inertia is zero, because of symmetry. So, the Eq. (8) can be rewritten as

$$\frac{\partial N_{xx}}{\partial x}+\frac{\partial N_{xy}}{\partial y}=0 \tag{18-a}$$

$$\frac{\partial N_{xy}}{\partial x}+\frac{\partial N_{yy}}{\partial y}=0 \tag{18-b}$$

$$\begin{aligned}&\frac{\partial^2M_{xx}}{\partial x^2}+2\frac{\partial^2M_{xy}}{\partial x\,\partial y}+\frac{\partial^2M_{yy}}{\partial y^2}+\frac{\partial}{\partial x}\left(N_{xx}\frac{\partial w_0}{\partial x}+N_{xy}\frac{\partial w_0}{\partial y}\right)\\&+\frac{\partial}{\partial y}\left(N_{xy}\frac{\partial w_0}{\partial x}+N_{yy}\frac{\partial w_0}{\partial y}\right)+q(x,y,t)=\mathrm{I}_0\frac{\partial^2w_0}{\partial t^2}\\&-I_2\frac{\partial^2}{\partial t^2}\left(\frac{\partial^2w_0}{\partial x^2}+\frac{\partial^2w_0}{\partial y^2}\right)\end{aligned} \tag{18-c}$$

The in-plane forces are defined as Eq. (19), using an Airy stress function ϕ and compatibility Eq. (20)

$$\begin{cases}N_{xx}=\dfrac{\partial^2\phi}{\partial y^2}\\N_{yy}=\dfrac{\partial^2\phi}{\partial x^2}\\N_{xy}=-\dfrac{\partial^2\phi}{\partial x\,\partial y}\end{cases} \tag{19}$$

$$\frac{\partial^2\varepsilon^0_{xx}}{\partial y^2}+\frac{\partial^2\varepsilon^0_{yy}}{\partial x^2}-\frac{\partial^2\varepsilon^0_{xy}}{\partial x\,\partial y}=\left(\frac{\partial^2w_0}{\partial x\,\partial y}\right)^2-\frac{\partial^2w_0}{\partial x^2}\frac{\partial^2w_0}{\partial y^2}. \tag{20}$$

Since the Eq. (20) is based on the strains, Eqs. (12) and (13) can be presented as Eq. (21)

$$\begin{aligned}&\begin{Bmatrix}\varepsilon^0\\M\end{Bmatrix}=\begin{bmatrix}A^*&B^*\\-(B^*)^T&D^*\end{bmatrix}\begin{Bmatrix}N\\\varepsilon^1\end{Bmatrix}\\&+\begin{bmatrix}A^*&O_{3\times3}\\-(B^*)^T&-I_{3\times3}\end{bmatrix}\begin{Bmatrix}N^T+N^e+N^m\\M^T+M^e+M^m\end{Bmatrix}\end{aligned} \tag{21}$$

where

$$\begin{cases}A^*=A^{-1}\\B^*=-A^{-1}B=O_{3\times3},O_{3\times3}=\begin{bmatrix}0&0&0\\0&0&0\\0&0&0\end{bmatrix},I_{3\times3}=\begin{bmatrix}1&0&0\\0&1&0\\0&0&1\end{bmatrix}\\D^*=\bar{D}-BA^{-1}B\end{cases} \tag{22}$$

By substituting Eqs. (19), (21) and (22) in Eqs. (18) and (20), following equations have been obtained

$$\begin{aligned}&\bar{D}_{11}\frac{\partial^2\varepsilon^1_{xx}}{\partial x^2}+\bar{D}_{12}\frac{\partial^2\varepsilon^1_{yy}}{\partial x^2}+\bar{D}_{12}\frac{\partial^2\varepsilon^1_{xx}}{\partial y^2}+\bar{D}_{22}\frac{\partial^2\varepsilon^1_{yy}}{\partial y^2}\\&+2\left(\bar{D}_{66}\frac{\partial^2\varepsilon^1_{xy}}{\partial x\,\partial y}\right)+\frac{\partial}{\partial x}\left(\frac{\partial^2\phi}{\partial y^2}\frac{\partial w_0}{\partial x}-\frac{\partial^2\phi}{\partial x\,\partial y}\frac{\partial w_0}{\partial y}\right)\\&+\frac{\partial}{\partial y}\left(-\frac{\partial^2\phi}{\partial x\,\partial y}\frac{\partial w_0}{\partial x}+\frac{\partial^2\phi}{\partial x^2}\frac{\partial w_0}{\partial y}\right)+q(x,y,t)\\&=\mathrm{I}_0\frac{\partial^2w_0}{\partial t^2}-I_2\frac{\partial^2}{\partial t^2}\left(\frac{\partial^2w_0}{\partial x^2}+\frac{\partial^2w_0}{\partial y^2}\right)\end{aligned} \tag{23}$$

$$\begin{aligned}&\frac{\partial^2}{\partial y^2}\left(A^*_{11}\frac{\partial^2\phi}{\partial y^2}+A^*_{12}\frac{\partial^2\phi}{\partial x^2}+A^*_{11}\left(N^T_{xx}+N^e_{xx}+N^m_{xx}\right)+A^*_{12}\left(N^T_{yy}+N^e_{yy}+N^m_{yy}\right)\right)+\\&\frac{\partial^2}{\partial x^2}\left(A^*_{12}\frac{\partial^2\phi}{\partial y^2}+A^*_{12}\frac{\partial^2\phi}{\partial x^2}+A^*_{12}\left(N^T_{xx}+N^e_{xx}+N^m_{xx}\right)+A^*_{22}\left(N^T_{yy}+N^e_{yy}+N^m_{yy}\right)\right)\\&+2A^*_{66}\frac{\partial^2}{\partial x\,\partial y}\left(\frac{\partial^2\phi}{\partial x\,\partial y}\right)=\left(\frac{\partial^2w_0}{\partial x\,\partial y}\right)^2-\frac{\partial^2w_0}{\partial x^2}\frac{\partial^2w_0}{\partial y^2}\end{aligned} \tag{24}$$

For deriving the Airy stress function and transverse deflection of the plate, it is necessary to determine boundary conditions. In this problem, simply supported with immovable edges have been considered as boundary conditions. So, the boundary conditions can be introduced as:

$$\begin{aligned}&w_0=v_0=M_{xx}=N_{xy}=0\quad\text{at } x=0,a\\&w_0=u_0=M_{yy}=N_{xy}=0\quad\text{at y}=0,b\end{aligned} \tag{25}$$

According to the boundary conditions (Eq. (25)), w0 can be defined as Eq. (26)

$$\begin{aligned}&w_0(x,y,t)=\sum_{n=1}^{\infty}\sum_{m=1}^{\infty}W_{mn}(t)F(x,y)=\\&\sum_{n=1}^{\infty}\sum_{m=1}^{\infty}W_{mn}(t)\sin\left(\frac{n\pi}{a}x\right)\sin\left(\frac{m\pi}{b}y\right)\end{aligned} \tag{26}$$

where m and n are mode number and $W_{mn}(t)$ indicates transverse time variant of the plate. Eq. (25) can be presented as following form

$$\begin{aligned}&v_0=\int\left(\varepsilon^0_{yy}-\frac{1}{2}\left(\frac{\partial w_0}{\partial y}\right)^2\right)dy=0,\qquad\text{at } x=0,a\\&u_0=\int\left(\varepsilon^0_{xx}-\frac{1}{2}\left(\frac{\partial w_0}{\partial x}\right)^2\right)dx=0,\qquad\text{at } y=0,b\\&\int_0^b N_{xy}dy=0\qquad\text{at } x=0,a\\&\int_0^a N_{xy}dx=0\qquad\text{at } y=0,b\end{aligned} \tag{27}$$

By determining the boundary conditions (Eq. (27)), the Eq. (24) can be solved now. So, airy function can be assigned by two particular (ϕ_p) and homogenous (ϕ_h) solutions

$$\phi=\phi_p+\phi_h \tag{28}$$

where

$$\phi_p = \widehat{\varphi}_1 \cos\left(\frac{2n\pi}{a}x\right) + \widehat{\varphi}_2 \cos\left(\frac{2m\pi}{b}y\right),$$
$$\widehat{\varphi}_1 = \frac{a^2 m^2 W_{mn}^2(t)}{32 b^2 n^2 A_{22}^*} = \varphi_1 W_{mn}^2(t), \quad (29)$$
$$\widehat{\varphi}_2 = \frac{b^2 n^2 W_{mn}^2(t)}{32 a^2 m^2 A_{11}^*} = \varphi_2 W_{mn}^2(t).$$

and

$$\phi_h = c_1 x^2 + c_2 y^2$$
$$c_1 = G_1\left(A^*\right) W_{mn}^2(t) - \frac{1}{2}N_{yy}^T - \frac{1}{2}N_{yy}^e - \frac{1}{2}N_{yy}^m \quad (30)$$
$$c_2 = G_2\left(A^*\right) W_{mn}^2(t) - \frac{1}{2}N_{xx}^T - \frac{1}{2}N_{xx}^e - \frac{1}{2}N_{xx}^m$$

in which

$$\begin{cases} G_1\left(A^*\right) = -\dfrac{\pi^2}{16}\dfrac{a^2 m^2 A_{11}^* - b^2 n^2 A_{12}^*}{a^2 b^2\left(A_{12}^{*2} - A_{11}^* A_{22}^*\right)} \\ G_2\left(A^*\right) = \dfrac{\pi^2}{16}\dfrac{a^2 m^2 A_{12}^* - b^2 n^2 A_{22}^*}{a^2 b^2\left(A_{12}^{*2} - A_{11}^* A_{22}^*\right)} \end{cases} \quad (31)$$

For abbreviation, $W_{mn}(t)$ is just indicated by W. Finally using Galerkin method and known Airy stress function (Eq. (28)), the Eq. (23) has been converted into an Ordinary Differential Equations (ODE) as

$$Z_1 \ddot{W}(t) + Z_2 W(t) + Z_3 W^2 + Z_4 W^3(t) + Z_5 W(t) V_e(t) + Z_6 W(t) I_m(t) + Z_7 q(t) = 0 \quad (32)$$

where Z_i, i=1-7, are constant coefficients which are shown in appendix A, and q is external excitation and W is time variant transverse displacement of the plate. The terms $Z_5 W(t) V_e(t)$ and $Z_6 W(t) I_m(t)$ are the coupling terms of electric voltage and induced current.

When the structure is symmetric, the Z_3 is equal to zero. Because the Eq. (32) has three unknown variables, $V_e(t)$, $I_m(t)$ and $W(t)$, two other equations are necessary to solve them simultaneously. The other equations are extracted from electrical and magnetic aspects of the behavior of the structure.

2- 3- Electromagnetic modeling of the plate

The deflection of a magnetoelectroelastic structure leads to produce electric and magnetic fields. The following presented model is suggested to introduce the governing equations for electrical and magnetic parts of a MEE harvester. According to Eq. (4b), the strain of the plate leads to the electric displacement. Since, the external circuit admittance across the electrodes is $1/R$, the output current can be obtained by integral form of the Gauss law, [22]. According to The Gauss law, the charge density over piezoelectric layers is equal to electric displacement field between the electrodes. Electric current could be explained by derivation of electric charge as

$$I_e(t) = \frac{d}{dt}\left(\int_A D_z . \mathrm{n} dA\right) \quad (33)$$

where D_z is electric displacement in the thickness direction of the plate and n is external normal vector [23]. According to Eq. (4b), D_z can be expanded in below form

$$D_z = e_{31}\left(\varepsilon_{xx}^0 + z\,\varepsilon_{xx}^1 - \alpha_1 \Delta T\right) + e_{32}\left(\varepsilon_{yy}^0 + z\,\varepsilon_{yy}^1 - \alpha_2 \Delta T\right) + \in_{33} E_z + d_{33} H_z . \quad (34)$$

Since, the positions of two MEE layers in z-direction are at top and bottom of the plate, regarding the fact that z is the distance between the mid-plane and the center of each MEE layer (h_{is}=(h_s+h_i)/2), by substituting Eq. (33) in Ohm law one obtains:

$$\frac{d}{dt}\left(\int_A D_z . \mathrm{n} dA\right)_{z=h_{is}} + \frac{d}{dt}\left(\int_A D_z . \mathrm{n} dA\right)_{z=h_{is}} = \frac{V_e}{R} \quad (35)$$

Substituting Eq. (34) in Eq. (35)

$$I_c + C_e \frac{dV_e}{dt} + T_1 \frac{dI_m}{dt} = \frac{V_e}{R} \quad (36)$$

where I_c and C_e are constant current source and capacitance, respectively. Also dI_m/dt is voltage-controlled current source and T_1 is constant coefficient. According to Eq. (8), the equivalent circuit of the electro-mechanical part of a MEE harvester can be shown as Fig. 2.

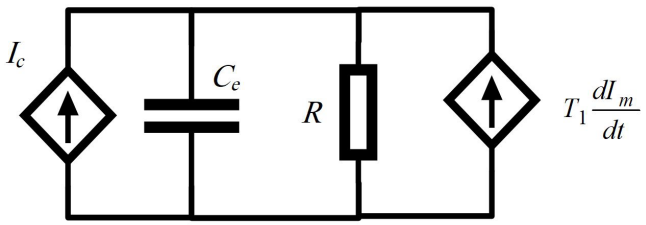

Fig. 2. Equivalent circuit of the electro-mechanical part of a MEE harvester.

In addition, the Eq. (4c) shows that the produced strain of the plate leads to the magnetic flux density, as well. Regarding the fact that the external circuit impedance across the electrodes is R, the output voltage can be obtained by integration form of Faraday's law [24]. The produced voltage of magnetic part of the harvester can be defined as below similar to Eq. (35),

$$V_m(t) = -\frac{d}{dt}\left(\int_A B_z . \mathrm{n} dA\right)_{z=h_{is}} - \frac{d}{dt}\left(\int_A B_z . \mathrm{n} dA\right)_{z=h_{is}} . \quad (37)$$

In the above equations, B_z is magnetic flux density in the thickness direction of the plate. According to Eq. (4c), can be expanded as

$$B_z = q_{31}\left(\varepsilon_{xx}^0 + |z|\,\varepsilon_{xx}^1 - \alpha_1 \Delta T\right) + q_{32}\left(\varepsilon_{yy}^0 + |z|\,\varepsilon_{yy}^1 - \alpha_2 \Delta T\right) + d_{33} E_z + \mu_{33} H_z . \quad (38)$$

Substituting Eq. (38) in Eq. (37) and using Ohm law, one can obtain

$$V_L + T_2 \frac{dV_e}{dt} + L_m \frac{dI_m}{dt} = RI_m \tag{39}$$

where V_L and L_m are constant voltage source and inductance, respectively, and dV_e/dt is current-controlled voltage source and T_2 is constant coefficient. As a result, according to Eq. (39), the equivalent circuit of the magneto-mechanical part of a MEE harvester can be shown as Fig. 3.

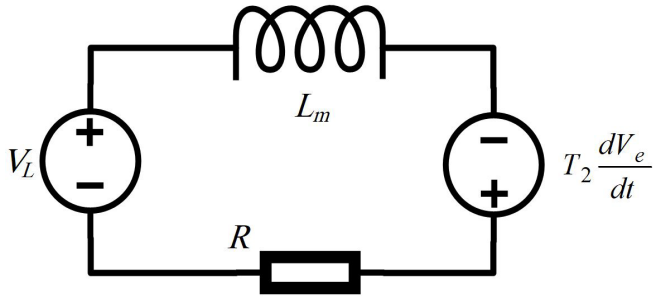

Fig. 3. Equivalent circuit of the magneto-mechanical part of a MEE harvester.

3- Solution of Coupled Equations

According to the previous section, we rewrite the ODE Eqs. (32) and (36) and (39), for transverse displacement and electrical and magnetic fields of the structure, respectively in the following form:

$$\begin{aligned}&\ddot{W}(t) + \omega^2 W(t) + 2\mu'\dot{W}(t) + s_2 W^3(t) \\ &+ s_3 W(t) V_e(t) + s_4 W(t) I_m(t) + s_5 q(t) = 0,\end{aligned} \tag{40}$$

$$\dot{V}_e(t) + J_1 \dot{I}_m(t) + J_2 V_e(t) + J_3 \dot{W}(t) + J_4 W(t)\dot{W}(t) = 0, \tag{41}$$

$$\dot{I}_m(t) + J_5 \dot{V}_e(t) + J_6 I_m(t) + J_7 \dot{W}(t) + J_8 W(t)\dot{W}(t) = 0. \tag{42}$$

The Eqs. (41) and (42) are the expanded form of the Eqs. (36) and (39), in which J_i for j=1-8 are the constant coefficients and the other coefficients in Eq. (40) are defined as

$$\omega = \sqrt{\frac{Z_2}{Z_1}}, s_2 = \frac{Z_4}{Z_1}, s_3 = \frac{Z_5}{Z_1}, s_4 = \frac{Z_6}{Z_1}, s_5 = \frac{Z_7}{Z_1} \tag{43}$$

The parameter μ' has been added to the Eq. (32) due to air damping and is defined as Eq. (44), and $q(t)$ is harmonic excitation force that is defined by Eq. (45).

$$\mu' = \zeta\omega. \tag{44}$$

$$q(t) = q_0 \cos(\omega_e t). \tag{45}$$

where ζ is damping coefficient. ω_e is excitation frequency and q_0 is excitation amplitude distributed uniformly over the plate surface.

By defining new dimensionless variables, T and U

$$T = \omega t \tag{46}$$

$$W = hU \tag{47}$$

By substituting derivative operators, $D=d/dT$ and $D^2=d^2/dT^2$, in the Eqs. (41) and (42), and solving them with respect to V_e and I_m, one can obtain:

$$\begin{aligned}&\frac{d^2U}{dT^2} + U + 2\tilde{\mu}\frac{dU}{dT} + \tilde{S}_2 U^3 + \tilde{S}_3 U V_e \\ &+ \tilde{S}_4 U I_m + \tilde{S}_5 q_0 \cos(\Omega T) = 0\end{aligned} \tag{48}$$

$$\begin{aligned}&\frac{d^2V_e}{dT^2} + P_1\frac{dV_e}{dT} + P_2 V_e = \\ &-P_3\left(J_3 h\frac{d^2U}{dT^2} + J_4 h^2\left(\left(\frac{dU}{dT}\right)^2 + U\frac{d^2U}{dT^2}\right)\right) \\ &-P_6\left(J_3 h\frac{dU}{dT} + J_4 h^2 U\frac{dU}{dT}\right) \\ &-P_7\left(J_7 h\frac{d^2U}{dT^2} + J_8 h^2\left(\left(\frac{dU}{dT}\right)^2 + U\frac{d^2U}{dT^2}\right)\right)\end{aligned} \tag{49}$$

$$\begin{aligned}&\frac{d^2I_m}{dT^2} + P_1\frac{dI_m}{dT} + P_2 I_m = \\ &-P_3\left(J_7 h\frac{d^2U}{dT^2} + J_8 h^2\left(\left(\frac{dU}{dT}\right)^2 + U\frac{d^2U}{dT^2}\right)\right) \\ &-P_4\left(J_7 h\frac{dU}{dT} + J_8 h^2 U\frac{dU}{dT}\right) \\ &-P_5\left(J_3 h\frac{d^2U}{dT^2} + J_4 h^2\left(\left(\frac{dU}{dT}\right)^2 + U\frac{d^2U}{dT^2}\right)\right)\end{aligned} \tag{50}$$

where

$$\begin{aligned}&\tilde{\mu} = \frac{\mu'}{\omega}, \tilde{S}_2 = \frac{h^2 s_2}{\omega^2}, \tilde{S}_3 = \frac{s_3}{\omega^2}, \tilde{S}_4 = \frac{s_4}{\omega^2}, \tilde{S}_5 = \frac{s_5}{h\omega^2}, \Omega = \frac{\omega_e}{\omega} \\ &P_1 = \frac{(J_2 + J_6)}{\omega(1 - J_1 J_5)}, P_2 = \frac{J_2 J_6}{\omega^2(1 - J_1 J_5)}, P_3 = \frac{1}{(1 - J_1 J_5)}, \\ &P_4 = \frac{J_2}{\omega(1 - J_1 J_5)} P_5 = \frac{-J_5}{(1 - J_1 J_5)}, P_6 = \frac{J_6}{\omega(1 - J_1 J_5)}, \\ &\tilde{P}_7 = \frac{-J_1}{(1 - J_1 J_5)}\end{aligned} \tag{51}$$

The Eqs. (48) to (50) will be solved using multiple time scales method. Eq. (48) is rewritten as a standard Duffing equation by assuming small parameter λ [25]. All terms are updated using booking parameter λ for introducing weakly nonlinearity [26], so the nonlinear mechanical Eq. (48) is rewritten as follows

$$\frac{d^2U}{dT^2}+U+\lambda\left(2\mu\frac{dU}{dT}+U^3+S_3UV_e+S_4UI_m+S_5q_0\cos(\Omega T)\right)=0 \tag{52}$$

in which

$$\lambda=\tilde{S}_2,\ \mu=\frac{\tilde{\mu}}{\lambda},\ S_3=\frac{\tilde{S}_3}{\lambda},\ S_4=\frac{\tilde{S}_4}{\lambda},\ S_5=\frac{\tilde{S}_5}{\lambda} \tag{53}$$

In case of primary resonance, the excitation frequency may be rewritten as follows

$$\Omega=1+\tilde{\sigma}\lambda \tag{54}$$

where $\tilde{\sigma}$ is detuning parameter. By defining time scales in Eq. (55), derivative operators in Eq. (56) and U as Eq. (57)

$$\begin{cases}T_0=t\\T_1=\lambda t\end{cases} \tag{55}$$

$$\begin{cases}D_0=\dfrac{d}{dT_0}\\D_1=\dfrac{d}{dT_1}\end{cases}\Rightarrow\begin{cases}\dfrac{d}{dT}=D_0+\lambda D_1\\\dfrac{d^2}{dT^2}=D_0^2+2\lambda D_0D_1\end{cases} \tag{56}$$

$$U=U_0+\lambda U_1 \tag{57}$$

Applying above variables in Eqs. (49) and (50) and (52), and separated the equations developing by the coefficients of λ^0 and λ^1 , the solutions for U, V_e and I_m are achieved. The coefficients for λ^0 is

$$D_0^2U_0+U_0=0 \tag{58}$$

$$\begin{aligned}&D_0^2V_e+P_1D_0V+P_2V_e=\\&-P_3\left(J_3h\left(D_0^2U_0\right)+J_4h^2\left(\left(D_0U_0\right)^2+U_0\left(D_0^2U_0\right)\right)\right)\\&-P_6\left(J_3h\left(D_0U_0\right)+J_4h^2U_0\left(D_0U_0\right)\right)\\&-P_7\left(J_7h\left(D_0^2U_0\right)+J_8h^2\left(\left(D_0U_0\right)^2+U_0\left(D_0^2U_0\right)\right)\right)\end{aligned} \tag{59}$$

$$\begin{aligned}&D_0^2I_m+P_1D_0I_m+P_2I_m=\\&-P_3\left(J_7h\left(D_0^2U_0\right)+J_8h^2\left(\left(D_0U_0\right)^2+U_0\left(D_0^2U_0\right)\right)\right)\\&-P_4\left(J_7h\left(D_0U_0\right)+J_8h^2U_0\left(D_0U_0\right)\right)\\&-P_5\left(J_3h\left(D_0^2U_0\right)+J_4h^2\left(\left(D_0U_0\right)^2+U_0\left(D_0^2U_0\right)\right)\right)\end{aligned} \tag{60}$$

The solution of Eq. (58) has been obtained as

$$U_0=A_0\left(T_1\right)e^{iT_0}+cc. \tag{61}$$

where A_0 is the amplitude of U_0 depending on T_1 and cc is complex conjugate of prior terms in the equation. Substituting Eq. (61) in Eqs. (59) and (60) have been obtained as

$$D_0^2V_e+P_1D_0V+P_2V_e=P_8A_0e^{iT_0}+P_9A_0^2e^{2iT_0}+cc \tag{62}$$

$$D_0^2I_m+P_1D_0I_m+P_2I_m=P_{10}A_0e^{iT_0}+P_{11}A_0^2e^{2iT_0}+cc \tag{63}$$

in which

$$\begin{aligned}&P_8=\left(P_3J_3+P_7J_7\right)h-iP_6J_3h,\ P_9=-2\left(P_3J_4+P_7J_8\right)h^2-iP_6J_4h^2\\&P_{10}=\left(P_3J_7+P_5J_3\right)h-iP_4J_7h,\ P_{11}=-2\left(P_3J_8+P_5J_4\right)h^2-iP_4J_8h^2\end{aligned} \tag{64}$$

The transient solution of Eqs. (62) and (63) can ignored and steady state solution only considered which is obtained as:

$$V_e=V_e^p=P_{12}A_0e^{iT_0}+P_{13}A_0^2e^{2iT_0}+cc \tag{65}$$

$$I_m=I_m^p=P_{14}A_0e^{iT_0}+P_{15}A_0^2e^{2iT_0}+cc. \tag{66}$$

in which

$$\begin{aligned}&P_{12}=\frac{P_8\left(\left(P_2-1\right)-iP_1\right)}{\left(P_2-1\right)^2+P_1^2},\ P_{13}=\frac{P_9\left(\left(P_2-4\right)-i2P_1\right)}{\left(P_2-4\right)^2+4P_1^2}\\&P_{14}=\frac{P_{10}\left(\left(P_2-1\right)-iP_1\right)}{\left(P_2-1\right)^2+P_1^2},\ P_{15}=\frac{P_{11}\left(\left(P_2-4\right)-i2P_1\right)}{\left(P_2-4\right)^2+4P_1^2}\end{aligned} \tag{67}$$

By considering the coefficients of λ^1 in Eq. (52) equal to zero, the following equation can be obtained.

$$\begin{aligned}&D_0^2U_1+U_1=-2D_0D_1U_0-2\mu D_0U_0\\&+U_0^3+S_3U_0V_e+S_4W_0I_m+S_5q,\end{aligned} \tag{68}$$

Substituting Eqs. (61) and (65) and (66) in Eq. (68) we have

$$\begin{aligned}D_0^2U_1+U_1=&-\left(1+S_3P_{13}+S_4P_{15}\right)A_0^3e^{3iT_0}\\&-\left(2i\left(D_1A_0\right)+2i\mu A_0+3A_0^2\overline{A}_0+S_3A_0^2\overline{A}_0P_{15}+S_4A_0^2\overline{A}_0P_{13}+\frac{S_5q_0}{2}e^{i\sigma T_1}\right)e^{iT_0}\\&-\left(S_3P_{12}+S_4P_{14}\right)A_0\overline{A}_0+cc\end{aligned} \tag{69}$$

In the above equations, the coefficient of e^{iT_0} leads to instability. Therefore, to obtain the stable solution, these coefficients which are known as secular terms, must be omitted. As a result, the solvability condition for this equation is

$$\begin{aligned}&2i\left(D_1A_0\right)+2i\mu A_0+3A_0^2\overline{A}_0+S_3A_0^2\overline{A}_0P_{15}\\&+S_4A_0^2\overline{A}_0P_{13}+\frac{S_5q_0}{2}e^{i\sigma T_1}\end{aligned} \tag{70}$$

By assuming the polar form for A_0 as $A_0=1/2k(T_1)e^{\beta(T_1)}$, in which k is response amplitude and β is the phase of A_0.

$$i\left(k'+ik\beta'+\mu k\right)+\frac{1}{8}\left(3+S_3P_{13}+S_4P_{15}\right)k^3+\frac{S_5q_0}{2}e^{i(\sigma T_1-\beta)}=0 \tag{71}$$

where k' and β' are the derivative of k and β with respect to T_1. Separating real and imaginary parts in Eq. (71)

$$\begin{cases} k' + \mu k + \frac{1}{8}\left(S_3 P_{13i} + S_4 P_{15i}\right)k^3 = -\frac{S_5 q_0}{2}\sin\left(\tilde{\sigma} T_1 - \beta\right) \\ -k\beta' + \frac{1}{8}\left(3 + S_3 P_{13r} + S_4 P_{15r}\right)k^3 = -\frac{S_5 q_0}{2}\cos\left(\tilde{\sigma} T_1 - \beta\right) \end{cases} \quad (72)$$

the subscripts i and r indicate to the imaginary and real part of related coefficients. Introducing $\gamma=(\tilde{\sigma}T_1-\beta)$, and considering steady state solution meaning $k'=\gamma'=0$, then

$$\begin{cases} \mu k + \frac{1}{8}\left(S_3 P_{13i} + S_4 P_{15i}\right)k^3 = -\frac{S_5 q_0}{2}\sin\gamma \\ -k\tilde{\sigma} + \frac{1}{8}\left(3 + S_3 P_{13r} + S_4 P_{15r}\right)k^3 = -\frac{S_5 q_0}{2}\cos\gamma \end{cases} \quad (73)$$

Ultimately, the analytical frequency response functions for the harvester have been obtained as

$$\begin{aligned} &\left(\mu k + \frac{1}{8}\left(S_3 P_{13i} + S_4 P_{15i}\right)k^3\right)^2 \\ &+\left(-k\tilde{\sigma} + \frac{1}{8}\left(3 + S_3 P_{13r} + S_4 P_{15r}\right)k^3\right)^2 = \left(\frac{S_5 q_0}{2}\right)^2 \\ &\tan\beta = \frac{\mu k + \frac{1}{8}\left(S_3 P_{13i} + S_4 P_{15i}\right)k^3}{-k\tilde{\sigma} + \frac{1}{8}\left(3 + S_3 P_{13r} + S_4 P_{15r}\right)k^3} \end{aligned} \quad (74)$$

Using the above equations, one can obtain the amplitude of steady state solution of the structure in each frequency of excitation. So the following electric voltage and induced current from the harvester due to the vibration can be obtained using Eqs. (65) and (66) which are represented as

$$\begin{aligned} V_e &= P_{12r}k\cos\left((1+\tilde{\sigma}\lambda)T-\gamma\right) - P_{12i}k\sin\left((1+\tilde{\sigma}\lambda)T-\gamma\right) \\ &+\frac{1}{2}\left[P_{13r}k^2\cos\left(2\left((1+\tilde{\sigma}\lambda)T-\gamma\right)\right) + P_{13i}k^2\sin\left(2\left((1+\tilde{\sigma}\lambda)T-\gamma\right)\right)\right], \\ I_m &= P_{14r}k\cos\left(\left((1+\tilde{\sigma}\lambda)T-\gamma\right)\right) - P_{14i}k\sin\left(\left((\omega+\tilde{\sigma}\lambda)T-\gamma\right)\right) \\ &+\frac{1}{2}\left[+P_{15r}k^2\cos\left(2\left((1+\tilde{\sigma}\lambda)T-\gamma\right)\right) + P_{15i}k^2\sin\left(2\left((1+\tilde{\sigma}\lambda)T-\gamma\right)\right)\right]. \end{aligned} \quad (75)$$

The output power is also defined as the average summation of electrical and magnetic power in a linear period that is defined as:

$$Power = \frac{1}{2\pi}\int_0^{\frac{1}{2\pi}} \frac{1}{2}\left(RI_m^2 + \frac{V_e^2}{R}\right)dT \quad (76)$$

4- Optimization

Using the analytical relations for electric voltage and induced current, the power relation in Eq. (76) is considered as the cost function, and implementing optimization applying genetic algorithm method, one can find the optimum parameters to find maximum harvested power. In this study, a set of three parameters have been considered as a chromosome and optimized by genetic algorithm. The parameters are dimensionless ratio ($g=a/h$), load resistance (R) and detuning parameter (σ), while the cost function is output power Eq. (76). The operators of genetic algorithm are selection, crossover and mutation. In the selection operator, some pair chromosomes have been chosen by considering their cost, so that the more the cost of chromosome is the more the probability of selecting is. After selecting the pair chromosomes, these pair chromosomes, as parents, have been combined together and constitute other pair chromosomes, as children, while the parameters of the children have common features with their parents. When the crossover operation completes, a small percentage of new chromosomes has been selected randomly for mutation operation. In mutation operation, one of the parameters of the chromosome have been selected randomly and changed. The steps of optimization are detailed in [27, 28] and the its process is represented as Fig. 4.

5- Numerical Examples

Three numerical examples of energy harvesting of vibration of a MEE plate are studied for first mode, $m=n=1$. The examples have been run in optimized and un-optimized ways. In the first example, the validity of the model has been explored. The other problem has been investigated by three different materials: Barium Titanate ($BaTiO_3$) as a piezoelectric, Cobalt iron ferrite ($CoFe_2O_4$) as a piezomagnetic and the composite of these two materials (50 percent $BaTiO_3$ – 50

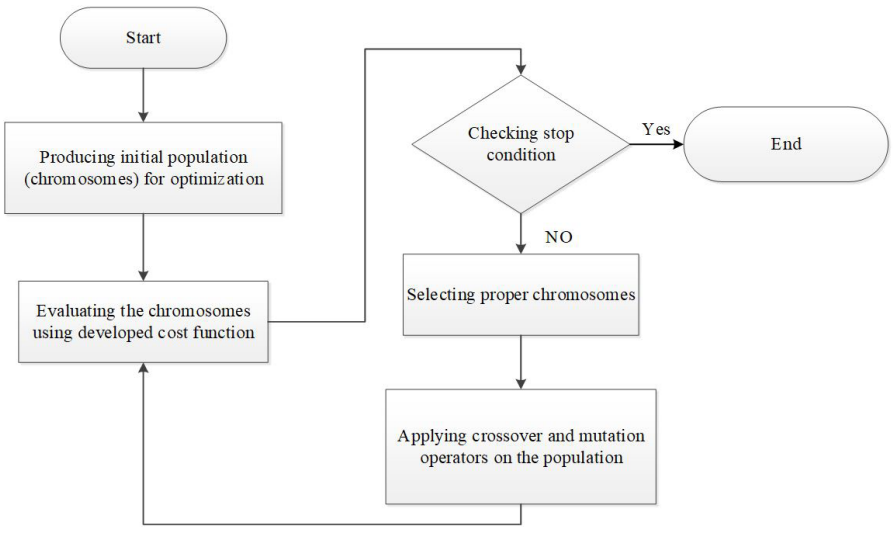

Fig. 4. The flowchart of the optimization

percent $CoFe_2O_4$) as a magneto-electro-elastic. The results are compared together. The properties of the smart materials are listed in Table 1. Also, the properties of the substructure is listed in Table 2.

5- 1- Verification of the model

Since the key purpose in this paper is to obtain an analytical relation for output power of the nonlinear vibration of a MEE plate, so it is necessary to validate the governing equation of motion (Eqs. (40) to (42)). For that reason, first, a FEM model in COMSOL Multiphysics software has been produced to compare it with numerical solution of the equations. In the next step, the comparison has been implemented between the results of numerical solution with those of multiple scale solution for electric voltage and induced current (Eq. (75)) of the next example.

5- 2- Finite element modeling

A three layered harvester, made from two Barium Titanate ($BaTiO_3$) material as a MEE layer at the top and bottom of graphite/epoxy material as substructure layer, has been designed in COMSOL Multiphysics software same as Fig. 1. Fig. 5 shows the FEM of the harvester. The required parameters of the plate is listed in Table 3.

It must be noticed that the developed model by COMSOL solves the problem in linear mode. That is, for comparing COMSOL results with those of numerical solution, the terms W3 and in Eqs. (40) to (42) must be considered to zero.

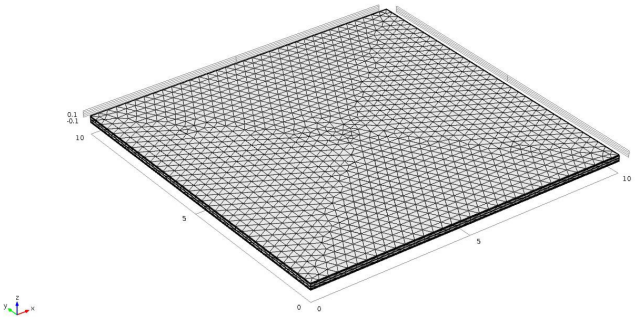

Fig. 5. The modeled plate in COMSOL

5- 3- Results from FEM model

The distribution of stress on the plate is shown in Fig. 6. The first mode deformation of the plate is observed in this figure. Also, we can see that the center and the corners of the plate are undergoing the biggest amount of stress. Fig. 7 shows the displacement of the center point of the plate in the FE model and numerical solution (Runge–Kutta) of the Eqs. (40) to (42). It is seen that the period of the vibration has good agreement with the FE model. The amplitude also has a reliable precision. Also, Fig. 8 shows the extracted voltage of the plate versus time, obtained by numerical solution of the Eqs. (40) to (42) and FEM. The extracted voltage accuracy has the same trend as the center point displacement of the plate.

Table 1. Smart materials properties [29]

Symbol	Unit	Parameter	Value		
			$BaTiO_3$- $CoFe_2O_4$	$BaTiO_3$	$CoFe_2O_4$
ρ	kg/m^3	Density	5550	5800	5300
α	1/^{o}C	Expansion coefficient	12.2e-6	11.3e-6	11e-6
Q_{11}	N/m^2	Elasticity modulus	213e9	166e9	286e9
Q_{12}	N/m^2	Elasticity modulus	113e9	77e9	173e9
Q_{66}	N/m^2	Elasticity modulus	49.9e9	43e9	45.3e9
e_{31}	C/m^2	Piezoelectric coefficient	-2.71	-4.4	0
e_{32}	C/m^2	Piezoelectric coefficient	-2.71	-4.4	0
q_{31}	N/A.m	Piezomagnetic coefficient	222	0	580
q_{32}	N/A.m	Piezomagnetic coefficient	222	0	580
ϵ_{33}	C/V	Dielectric modulus	6.37e-9	12.6e-9	0.093e-9
d_{33}	s/m	Electromagnetic coefficient	2750e-12	0	0
μ_{33}	N/A^2	Permeability	83.9e-6	1e-6	157

Table 2. Properties of Graphite/Epoxy [20]

Symbol	Unit	Parameter	Value
ρ_s	kg/m^3	Density	1581
α_{s11}			1.67 e-7
α_{s22}	1/^{o}C	Thermal expansion coefficient	156 e-7
α_{s33}			0
E_{s11}			139.89e9
E_{s22}	N/m^2	Elasticity modulus	10.576e9
G_{s12}			5.6537e9
v_{s12}	1	Poisson's ratio	0.24

Table 3. The parameters of the plate for verification.

Symbol	Unit	Name	Value
a	m	Plane dimension	0.01
b	m	Plane dimension	0.01
q_0	N/m^2	Excitation amplitude	10000
ω_e	Hz	Excitation frequency	90000
h_i	mm	Smart material thickness	0.0033
h_s	mm	Substructure thickness	0.0133
R	Ohm	Resistance load	50

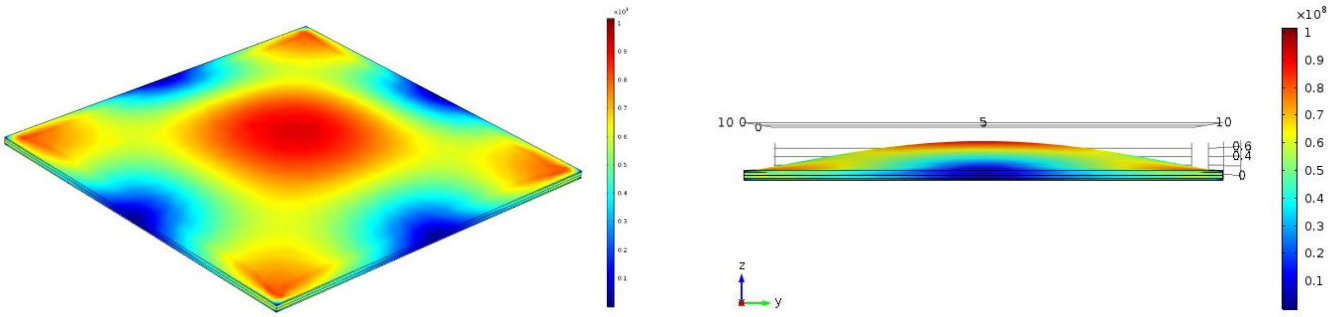

Fig. 6. Distribution of stress on the plate (isometric and lateral views)

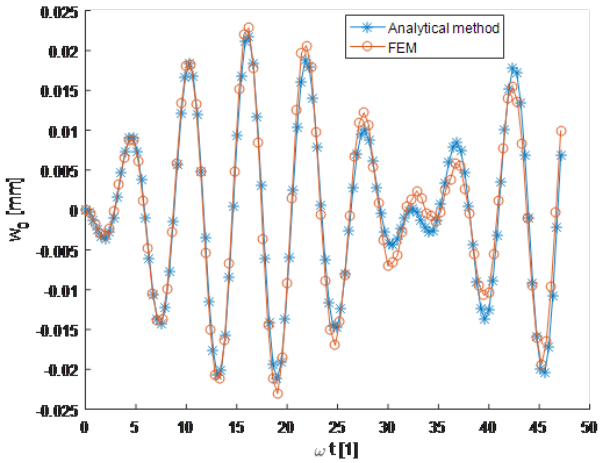

Fig. 7. Displacement of the center point of the plate obtained using numerical solution and FEM

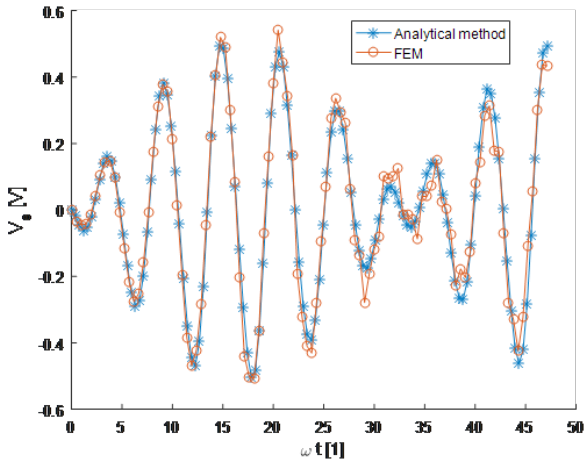

Fig. 8. Extracted voltage of the plate obtained using numerical solution and FEM

The above figures show that the derived model (Eqs. (40) to (42)) has been validate by FEM, because two diagrams confirm each other with proper accuracy.

5- 4- Optimized example

In this section, the effect of the parameters on the power, after optimization, are investigated. The parameters (Eq. (77)) are considered as chromosome of genetic algorithm and have been optimized for each smart material, separately, so we can compare the materials in their best versions. Since the derivation of motion of plate is based on the Kirchhoff plate theory, the side to thickness ratio, g, must be bigger than 20. Also, the multiple time scale method, should be used when side to thickness ratio is smaller than 50, because for the side to thickness ratio bigger than 50 the solution is diverging. For this purpose, the parameters are limited as Eq. (78)

$$C_0 = \begin{bmatrix} g & R & \sigma \end{bmatrix} \tag{77}$$

$$\begin{cases} 20 < g < 50 \\ 1 < R < 5\times 10^4 \\ -10^4 < \sigma < 10^4 \end{cases} \tag{78}$$

where $g=a/h$ is side to thickness ratio, R is load resistance, σ is detuning parameter that indicates the frequency and can be calculated by $\sigma=\tilde{\sigma}/\omega$. In this example, $a=b$=0.1m, and q_0=1000 N/m^2.

The parameters of each structure are optimized by genetic algorithm. The optimized parameters are listed as follows

$$C_0 = \begin{cases} \begin{bmatrix} 50 & 25 & 38 \end{bmatrix} & \text{for } CoFe_2O_4 \\ \begin{bmatrix} 50 & 215 & 79 \end{bmatrix} & \text{for } BaTiO_3 \\ \begin{bmatrix} 50 & 13 & 55 \end{bmatrix} & \text{for } BaTiO_3\text{-}CoFe_2O_4 \end{cases} \tag{79}$$

The harvested power, during a linear period, for these optimized parameters is listed in Table 4.

According to Eq. (78), the optimized dimensionless ratio for the three structures are the same of on the upper bound.

By the way, according to Eq. (79), PZT needs more resistance load to show its best version. Also, PZT needs more detuning parameter (or more excitation frequency). Harvested power for the structures, shown in Table 4, proves that PZM generates the highest power in less time. The generated power by PZT is more than MEE, while it needs more time to harvest such value of the power.

Table 4. Harvested power according to parameters (50).

Smart Material	Linear Period (ms)	Harvested Power (mW)
$CoFe_2O_4$ (PZM)	0.7919	1420
$BaTiO_3$ (PZT)	1.0441	699.01
$BaTiO_3$ - $CoFe_2O_4$ (MEE)	0.913	586.5

To verify the obtained analytical solutions, the diagrams of electric voltage and induced current are compared with relations of Eq. (75) and the numerical solution of Eqs. (40) to (42). The numerical solution uses Runge-Kutta method and has been provided by MATLAB software. Figs. 9 and 10 show the comparison between steady state analytical (Eq. (75)) and numerical solution of electrical voltage and induced current, respectively, by the optimized parameters (Eq. (79)) for the MEE material. It is obvious that the presented analytical solution in Eq. (75) is almost equal to numerical solution. In the previous example, the extracted model in Eqs. (40) to (42) are verified by FEM simulation, and here is shown that multiple scale method works correctly for the presented model of a magneto-electro-elastic structure. Therefore, we can claim that the extracted model and solution for the MEE structure are properly correct.

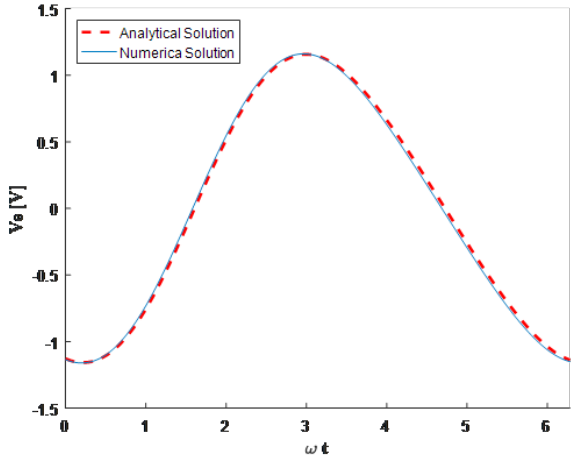

Fig. 9. Numerical and analytical electrical voltage during a linear period by optimized parameters of MEE in Eq. (79)

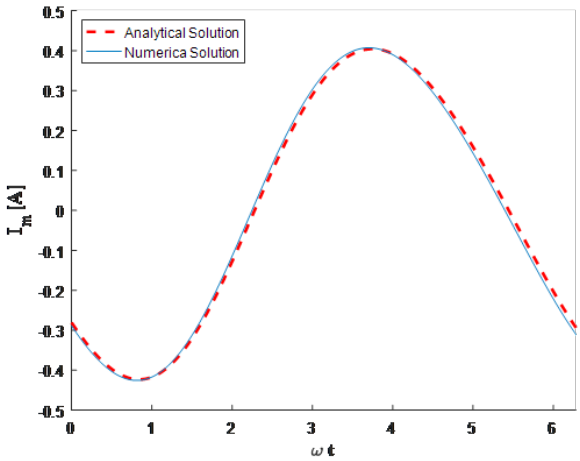

Fig. 10. Numerical and analytical induced current during a linear period by optimized parameters of MEE in Eq. (79)

According to optimized parameters in Eq. (79), the effect of the optimized parameters on the power are investigated. Fig. 11 shows the effect of side to thickness ratio on the output power when the other optimized parameters are constant. The peak point for all structures occurs in the upper bound of the limitation (Eq. (78)). The advantage of the PZM compared to the other structures is clear, here. Fig. 12 shows the effect of the resistance on the output power. It is clear that the power almost has same trend in different structures. All structures have a peak and approach to zero in infinity except MEE structure that has two peaks. It is seen that PZM has more power in low values of the resistance, and PZT has more power in high values of the resistance. Also, after passing from the initial values of the resistance, the effect of the resistance on the power in MEE is less than the other two, and MEE curve changes more smoothly than the other two.

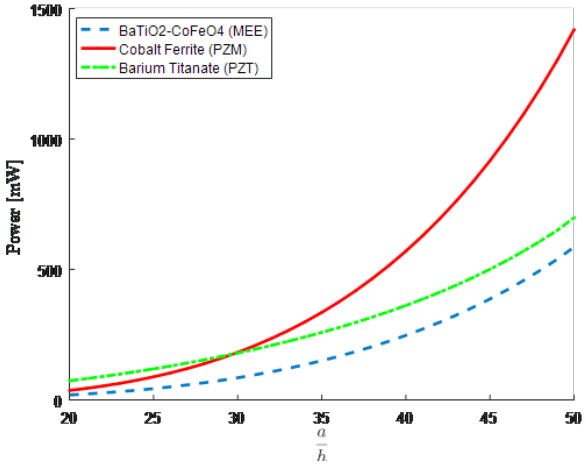

Fig. 11. Effect of dimensionless ratio on the power in optimized mode

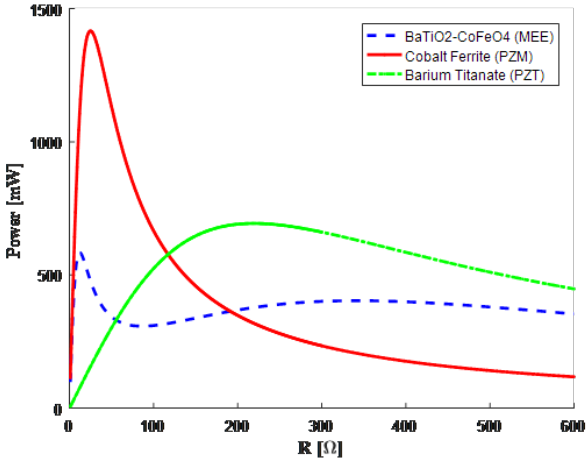

Fig. 12. Effect of the resistance on the power

Figs. 13 and 14 show the effect of the detuning parameter on the response amplitude and output power, respectively. We can see that the effect of detuning parameter on the response amplitude and power has the same trend in all kind of these three smart materials. Maximum power occurs when response amplitude is maximum. The backbone curve, the locus of peak amplitudes that depend on the damping coefficient value, is plotted in Fig. 13, as well.

6- Conclusion

In this paper, the nonlinear vibration energy harvesting from a MEE plate was studied. The MEE constituent equations with classical plate theory, von-Karman's nonlinear strain field,

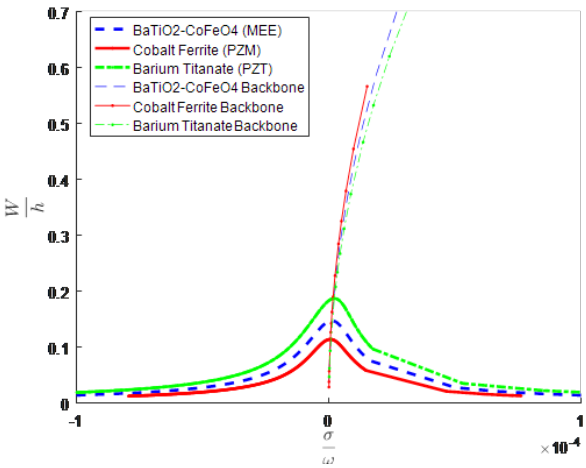

Fig. 13. Diagram of the detuning parameter versus response amplitude

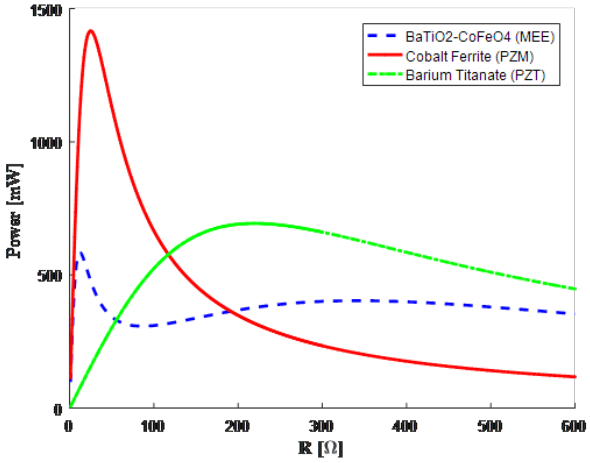

Fig. 14. Effect of the detuning parameter on the power

Gauss's law and Faraday's law were considered to develop the equations of motion of the harvester. Equivalent circuit of electrical and magnetic part of the structure is introduced. The analytical model is developed for a MEE vibration plate for the first time. These ODEs are solved by Multiple Scale method. After solving the equations, an analytical relation is obtained for the output power in a linear period, as well as the generated voltage by electrical part and induced current by magnetic part of the structure. The output power is used as cost function and the parameters of the structure are optimized by genetic algorithm.

An example for verifying the model and an example for illustrating the effectiveness of the developed model and optimization of the model has been studied by three different materials of PZT, PZM and MEE families. The extracted voltage and the displacement of the center point of the plate are verified by COMSOL with reliable accuracy. Optimization of the structure is performed for mentioned materials and it is observed that the optimal operation point for each material is different. According to the optimal operation point, the effect of different parameters on the power is studied and is compared for the materials. In comparison of three smart materials, it is found that if the structure made by these materials, run at their best version (optimized), PZM harvests the highest power while has the smaller linear period, as well, then PZT harvests more power than MEE. According to the diagram of the power against detuning parameter, PZM need less frequency to reach its maximum performance compared with MEE and specially PZT. Also, MEE load resistance is smaller than PZT and PZM. In terms of the harvested power, it is important to note that the structures have not the same condition with respect to each other in all values of the parameters. In some specific parameters, PZM generates more power than MEE and PZT, and sometimes MEE and PZT generate more power than PZM. The number and the length of the coils have a remarkable impact on the extracted power in MEE and especially in PZM. Also, the damping coefficient play a significant role in the harvested power, so using the correct value of damping coefficient helps to a better conclusion.

Appendix

The coefficients of the mechanical Eq. (32) are obtained as

$$
\begin{aligned}
Z_1 &= -\frac{1}{4ab}\left(I_2\pi^2\left(a^2m^2+b^2n^2\right)+I_0a^2b^2\right)\\
Z_2 &= -\frac{1}{4a^3b^3}\left(\pi^4\left(\bar{D}_{11}^{*}b^4n^4+2a^2b^2m^2n^2\left(\bar{D}_{12}^{*}+\bar{D}_{66}^{*}\right)+a^4m^4\bar{D}_{22}^{*}\right)\right.\\
&\quad \left.-\pi^2a^2b^2\left(n^2b^2N_{xx}^{e}+m^2a^2N_{yy}^{e}+n^2b^2N_{xx}^{m}+m^2a^2N_{yy}^{m}\right)\right)\\
Z_3 &= 0\\
Z_4 &= -\frac{1}{2}\frac{\pi^4}{ab}\left(m^2n^2\left(\varphi_1+\varphi_2\right)+G_1a^2m^2+G_2b^2n^2\right)\\
Z_5 &= -\frac{1}{4}\frac{\pi^2}{ab}\left(a^2m^2e_{32}+b^2n^2e_{31}\right)\\
Z_6 &= \frac{1}{4}\frac{N\pi^2h}{abl}\left(a^2m^2q_{32}+b^2n^2q_{31}\right)\\
Z_7 &= \begin{cases}4\dfrac{ab}{mn\pi^2}, & m,n=1,3,5,\ldots\\ 0, & m,n=2,4,6,\ldots\end{cases}
\end{aligned}
\tag{80}
$$

References

[1] C. Zhang, J. Yang, W. Chen, Harvesting magnetic energy using extensional vibration of laminated magnetoelectric plates, *Applied Physics Letters*, 95(1) (2009) 013511.

[2] C.J. Rupp, A. Evgrafov, K. Maute, M.L. Dunn, Design of piezoelectric energy harvesting systems: a topology optimization approach based on multilayer plates and shells, *Journal of Intelligent Material Systems and Structures*, 20(16) (2009) 1923-1939.

[3] C.D.M. Junior, A. Erturk, D.J. Inman, An electromechanical finite element model for piezoelectric energy harvester plates, *Journal of Sound and Vibration*, 327(1) (2009) 9-25.

[4] A. Erturk, J. Hoffmann, D. Inman, A piezomagnetoelastic structure for broadband vibration energy harvesting, *Applied Physics Letters*, 94(25) (2009) 254102.

[5] X. Dai, Y. Wen, P. Li, J. Yang, G. Zhang, Modeling, characterization and fabrication of vibration energy harvester using Terfenol-D/PZT/Terfenol-D composite

transducer, *Sensors and Actuators A: Physical*, 156(2) (2009) 350-358.

[6] K.H. Sun, Y.Y. Kim, Layout design optimization for magneto-electro-elastic laminate composites for maximized energy conversion under mechanical loading, *Smart Materials and Structures*, 19(5) (2010) 055008.

[7] A. Milazzo, C. Orlando, An equivalent single-layer approach for free vibration analysis of smart laminated thick composite plates, *Smart Materials and Structures*, 21(7) (2012) 075031.

[8] Z. Wu, R. Harne, K. Wang, Excitation-induced stability in a bistable Duffing oscillator: analysis and experiments, *Journal of Computational and Nonlinear Dynamics*, 10(1) (2015) 011016.

[9] M.M. El-Hebeary, M.H. Arafa, S.M. Megahed, Modeling and experimental verification of multi-modal vibration energy harvesting from plate structures, *Sensors and Actuators A: Physical*, 193 (2013) 35-47.

[10] S.C. Stanton, B.A. Owens, B.P. Mann, Harmonic balance analysis of the bistable piezoelectric inertial generator, *Journal of Sound and Vibration*, 331(15) (2012) 3617-3627.

[11] H. Talleb, Z. Ren, Finite element modeling of magnetoelectric laminate composites in considering nonlinear and load effects for energy harvesting, *Journal of Alloys and Compounds*, 615 (2014) 65-74.

[12] L.-L. Ke, Y.-S. Wang, Free vibration of size-dependent magneto-electro-elastic nanobeams based on the nonlocal theory, *Physica E: Low-dimensional Systems and Nanostructures*, 63 (2014) 52-61.

[13] S. Razavi, A. Shooshtari, Nonlinear free vibration of magneto-electro-elastic rectangular plates, *Composite Structures*, 119 (2015) 377-384.

[14] M.M. Shirbani, M. Shishesaz, A. Hajnayeb, H.M. Sedighi, Coupled magneto-electro-mechanical lumped parameter model for a novel vibration-based magneto-electro-elastic energy harvesting systems, *Physica E: Low-dimensional Systems and Nanostructures*, 90 (2017) 158-169.

[15] H. Shorakaei, A. Shooshtari, Analytical solution and energy harvesting from nonlinear vibration of an asymmetric bimorph piezoelectric plate and optimizing the plate parameters by genetic algorithm, *Journal of Intelligent Material Systems and Structures*, (2017) 1045389X17730919.

[16] V. Birman, *Plate structures*, Springer Science & Business Media, Netherlands, 2011.

[17] J.N. Reddy, *Mechanics of laminated composite plates and shells: theory and analysis*, CRC press, 2004.

[18] C.-Y. Chia, *Nonlinear analysis of plates*, McGraw-Hill International Book Company, 1980.

[19] H.-S. Shen, *Functionally graded materials: nonlinear analysis of plates and shells*, CRC press, 2016.

[20] J.N. Reddy, *Theory and analysis of elastic plates and shells*, CRC press, 2006.

[21] M. Rafiee, X. He, K. Liew, Nonlinear analysis of piezoelectric nanocomposite energy harvesting plates, *Smart Materials and Structures*, 23(6) (2014) 065001.

[22] A. Erturk, D.J. Inman, *Piezoelectric energy harvesting*, John Wiley & Sons, The Atrium, Southern Gate, Chichester, West Sussex, 2011.

[23] D.J. Griffiths, *Introduction to electrodynamics*, Prentice Hall, 93 (1999) 95.

[24] W.H. Hayt, J.A. Buck, *Engineering electromagnetics*, McGraw-Hill New York, 2001.

[25] T. Burton, Z. Rahman, On the multi-scale analysis of strongly non-linear forced oscillators, *International Journal of Non-Linear Mechanics*, 21(2) (1986) 135-146.

[26] A. Nayfeh, D. Mook, *Nonlinear Oscillations*, John Wiley and Sons, New York, (1979).

[27] H. Shorakaei, M. Vahdani, B. Imani, A. Gholami, Optimal cooperative path planning of unmanned aerial vehicles by a parallel genetic algorithm, *Robotica*, 34(04) (2016) 823-836.

[28] V. Azimirad, H. Shorakaei, Dual hierarchical genetic-optimal control: A new global optimal path planning method for robots, *Journal of Manufacturing Systems*, 33(1) (2014) 139-148.

[29] C.-X. Xue, E. Pan, On the longitudinal wave along a functionally graded magneto-electro-elastic rod, *International Journal of Engineering Science*, 62 (2013) 48-55.

Please cite this article using:

H. Shorakaei, A.R. Shooshtari, H.R. Karami, Analytical Solution and Optimization for Energy Harvesting from Nonlinear Vibration of Magneto- Electro- Elastic Plate, *AUT J. Mech. Eng.*, 3(1) (2019) 63-76.

DOI: 10.22060/ajme.2018.14453.5728